Properties of the anisotropy of dose contributions: A planning study on prostate cases

Johannes Greber,[a)] Bülent Polat, Michael Flentje, and Klaus Bratengeier
Department of Radiation Oncology, University of Würzburg, Josef-Schneider-Str. 11, 97080 Würzburg, Germany

(Received 11 April 2018; revised 23 October 2018; accepted for publication 7 November 2018; published 20 December 2018)

Purpose: To characterize the static properties of the anisotropy of dose contributions for different treatment techniques on real patient data (prostate cases). From this, we aim to define a class of treatment techniques with invariant anisotropy distribution carrying information of target coverage and organ-at-risk (OAR) sparing. The anisotropy presumably is a helpful quantity for plan adaptation problems.
Methods: The anisotropy field is analyzed for different intensity modulated radiotherapy (IMRT) and volumetric modulated arc therapy (VMAT) techniques for a total of ten planning CTs of prostate cases. Primary irradiation directions ranged from 5 to 15. The uniqueness of anisotropy was explored: In particular, the anisotropy distribution inside the planning treatment volume (PTV) and in its vicinity was investigated. Furthermore, deviations of the anisotropy under beam rotations were explored by direct plan comparison as an indicating the susceptibility of each planned technique to changes in the geometric plan configuration. In addition, plan comparisons enabled the categorization of treatment techniques in terms of their anisotropy distribution.
Results: The anisotropy profile inside the PTV and in the transition between OAR and PTV is independent of the treatment technique as long as a sufficient number of beams contribute to the dose distribution. Techniques with multiple beams constitute a class of almost identical and technique-independent anisotropy distribution. For this class of techniques, substructures of the anisotropy are particularly pronounced in the PTV, thus offering good options for applying adaptation rules. Additionally, the techniques forming the mentioned class fortunately allow a better OAR sparing at constant PTV coverage. Besides the characterization of the distribution, a pairwise plan comparison reveals each technique's susceptibility to deviations which decreases for an increasing number of primary irradiation directions.
Conclusions: Techniques using many irradiation directions form a class of almost identical anisotropy distributions which are assumed to provide a basis for improved adaptation procedures. Encouragingly, these techniques deliver quite invariant anisotropy distributions with respect to rotations correlated with good plan qualities than techniques using few gantry angles. The following will be the next steps toward anisotropy-based adaptation: first, the quantification of anisotropy regarding organ deformations; and second, establishing the interrelation between the anisotropy and beam shaping. © *2018 Universität Statnik Würzburg Germany. Medical Physics published by Wiley Periodicals, Inc. on behalf of American Association of Physicists in Medicine* [https://doi.org/10.1002/mp.13308]

Key words: adaptation, IMRT, radiotherapy, VMAT

1. INTRODUCTION

Imagine the common situation of a patient on the treatment table of the linear accelerator, whose volumetric modulated arc therapy (VMAT)[1,2] plan or intensity modulated radiotherapy (IMRT) plan has to be adapted along deformed anatomic structures within minutes or even seconds. These *ad hoc* adaptations are enabled by sophisticated image-guided radiation therapy (IGRT). Besides widely used methods like repositioning[3] and aperture tracking,[4] several methods have been developed which provide a smooth adaptation. These include reoptimizations[5] and dose deforming algorithms[6] which have also been applied for VMAT.[7] In recent years, the replacement of cone-beam CT imaging by magnetic resonance (MR) technology allows advances in soft tissue recognition. Thus, the previously considered ideas for *ad hoc* plan adaptation are particularly interesting for the next generation of linear accelerators, the MR-linac. Various fluence-based concepts for adaptive planning have been developed.[8–11] On the other side, the current state of MR-linac technology does not yet offer dynamic arcs and thus excludes VMAT.

In many cases, simply warping the fluence grid along projected organ contours in the beam's eye view (BEV) leads to satisfactory adaptation results. However, it has been shown that this method can fail under certain circumstances[12] since the usage of structure boundaries is connected to a loss of important three-dimensional (3D) information. This is explicitly the case for pronounced concave–convex planning treatment volume (PTV) and organ-at-risk (OAR) constellations.

The two-step adaptation method[12] reduces underdosages in the PTV by means of additional segments tangential to the OAR surface. It can avoid the problem of inadequate fluence grid warping, however, at the cost of increasing plan

complexity and numbers of arc rotations[13] Therefore, an indicator for the relevant 3D information that ideally may be applied to any treatment technique would be preferable. For this purpose, Bratengeier and Holubyev have suggested to use the anisotropy of dose contributions,[14] which is closely related to the two-step method. The anisotropy field has been analyzed in idealized geometries — a cylindrical OAR surrounded by a hollow cylindrical planning treatment volume (PTV). In addition, resulting anisotropy changes have been quantified for virtual deformations of the prostate and rectum. Furthermore, the necessary 3D information on OAR sparing is transferred into the PTV corpus. Therefore, it could be retrieved in the BEV in a way that is relevant for beam shape adaptation.

The purpose of this work is to take the first of three steps on the stairway to an anisotropy-assisted adaptation, and is presented in Table I. On each voxel, the anisotropy $\boldsymbol{A}$ is defined as sum over all irradiation directions n represented by the gantry angle γ_n, weighted by the dose-per-beam D_n of a finally optimized plan:

$$\boldsymbol{A} := \sum_n D_n(\cos 2\gamma_n, \sin 2\gamma_n) \tag{1}$$

with the effective direction γ

$$\gamma = \begin{cases} \frac{1}{2}\tan^{-1}\left(\frac{\sum_n D_n \sin 2\gamma_n}{\sum_n D_n \cos 2\gamma_n}\right) & \text{for } \sum_n D_n \cos 2\gamma_n \begin{cases} \geq 0 \\ < 0 \end{cases} \\ \frac{1}{2}\tan^{-1}\left(\frac{\sum_n D_n \sin 2\gamma_n}{\sum_n D_n \cos 2\gamma_n}\right) + \pi \end{cases} \tag{2}$$

pointing towards the main directions of dose contributions. This definition assumes similar effects of opposing irradiation directions: $\boldsymbol{A}(\gamma) = \boldsymbol{A}(\gamma + \pi)$. Furthermore, information on the target volume coverage and organ sparing is implicitly associated with this quantity due to the entering dose contributions, but might depend on the chosen coplanar beam directions, since the anisotropy relies on a two-dimensional definition.

To investigate the spatial dependence of anisotropy, a study on different inverse planned treatment techniques is considered, including IMRT techniques with different numbers of irradiation angles and a double-arc VMAT technique, which is assumed to be the most promising approach in terms of the plan quality.[15] For this, the anisotropy is calculated from the dose distribution obtained from ten planning CTs for a series of different treatment techniques, which differ in their number of irradiation directions, from 5 for IMRT to 90 for VMAT. These plans were analyzed in terms their anisotropy of dose contributions in dependence of the beam numbers. Considerations on the anisotropy distribution lead to at least two further questions concerning the anisotropy of dose contributions:

- To what extent can the anisotropy distribution be independent from the choice of the treatment technique, or in other words, is there a class of treatment techniques which leads to equal anisotropy distributions inside the PTV and its environment? (1.1. in Table I).
- Which techniques provide a stable anisotropy distribution with respect to instabilities like rotations of the treatment arrangement? (1.2. in Table I).

Although a plan improvement for an increasing number of irradiation directions has been shown in a simplified geometry and a certain setting of segmentation,[15] the quality of the various plan types has to be evaluated in connection with the anisotropy of dose contributions.

TABLE I. Research program.

Anisotropy of dose contributions to assist plan adaptation
1. Static properties
• Characterization of the anisotropy in the PTV vicinity
• Choice of well suited classes of techniques:
1. plan-independent anisotropy
2. anisotropy not prone to failures
• Anisotropy changes for differing OAR-PTV objectives
2. Dynamic properties (short overview)
• Quantitative changes for several types of deformations
• Prediction of changes of anisotropy from deformation of PTV- and OAR structures
3. Segment adaptation based on anisotropy deformation (short overview)
• Calculation of necessary segment shape changes from anisotropy deformations based on PTV- and OAR deformations
• Calculation of necessary leaf position shifts considering leaf motion limitations

2. MATERIALS AND METHODS

2.A. Anisotropy of dose contributions

The dose distribution $f(D)$ with its contributions D_n per beam n is calculated on a dose grid with grid constant of 3 mm in all three spatial dimensions. Dose distributions are calculated for IMRT with 5, 7, 11, and 15 beams. In addition, a double-arc VMAT plan was generated on a total of 10 planning CTs on prostate cases. For these plans, we demanded to fulfill clinical constraints. How good these constraints are met is given in Appendix A.

Bratengeier et al.[14] introduced a definition of an anisotropy field, which is given in Eqs. (1) and (2). Mathematically, this equation corresponds to a dose-per-beam weighted sum of irradiation directions, which takes into account the similar effect of two opposing irradiation direction γ_n and $\gamma_n + 180°$ by its 180° periodicity. The range of values is limited by $A = |\boldsymbol{A}| = D$ for a single beam and $A = 0$ for a completely isotropic or orthogonal irradiation. Therefore, data is normalized by the prescribed dose D_{mean} (cf. Fig. 1). An equally important mathematical property of Eqs. (1) and (2) is the vanishing anisotropy for orthogonal irradiation directions and equal dose contributions.

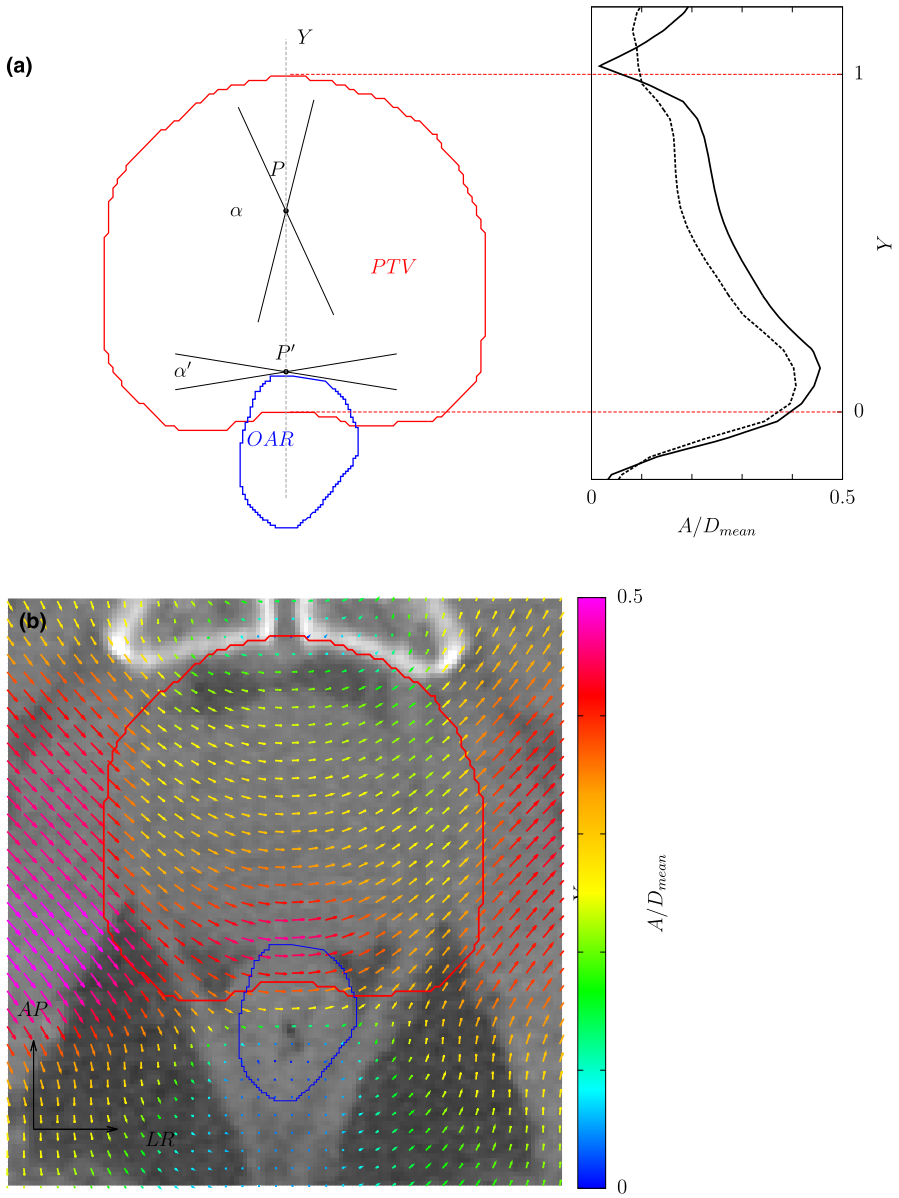

FIG. 1. (a) Considerations on the anisotropy at points P inside the PTV and P' close to an organ-at-risk (OAR). A reduced range α' of beam directions with strong dose contributions that do not pass the rectum yields anisotropy increase, as can be seen on the right, where anisotropy profiles $A(Y)$ obtained along the cross-section Y through PTV and rectum (gray-dashed line on the left) are depicted. Solid line: volumetric modulated arc therapy (VMAT); dashed line: seven-field DMPO plan. Red lines indicate the PTV surface. (b) Anisotropy $\boldsymbol{A}$ for a VMAT plan inside PTV and rectum. Length and color of each arrow correspond to the absolute value A, while it points towards the effective direction γ_{eff}. Particularly within the overlap region of PTV and rectum the anisotropy is tangential to the OAR.

The following point illustrates how the anisotropy may be uniquely useful for adaptation [cf. Fig. 1(a)]:

Here, two points P and P' inside the PTV with different distances to the OAR surface are depicted. For P, an almost isotropic dose deposition from a broad range α of directions is possible so that the anisotropy is small. In contrast, for P', only a small range α' of irradiation directions can contribute to the dose without traversing the OAR: anisotropy contributions reach their maximum. Additionally, a lateral broadening of the OAR will not be detected in the BEV for lateral beams. However, the angles α and α' will vary and therefore the anisotropy will change.

In both cases, the anisotropy changes in regions where the dose is required to be constant. Thus, we have to recognize that neither pure dose distributions nor BEV alone are sufficient for the indication of OAR tangential information for adaptation purposes.

Information on the organ sparing and target volume coverage is contained in the anisotropy profile within the PTV. This point is visualized exemplarily by the two anisotropy profiles tracked along the cross-section Y through the rectum and the PTV in Fig. 1(a). The depicted graphs result from data on two different treatment techniques. $Y = 0$ and $Y = 1$ indicate the PTV surface.

Similar shapes were predicted for the fluence $F(r)$ in radial direction r adjacent to the perfectly spared PTV-enclosed OAR in a rotationally symmetric phantom by Brahme et al.[16] Also there, the transition from isotropic to anisotropic irradiation played a significant role, since adjacent to the OAR, only tangential components contribute to the fluence: The scaling law

$$F(r) = \frac{F_0}{\sqrt{r}} \propto r^{-\frac{1}{2}} \tag{3}$$

was indicated.

The anisotropy explicitly depends on the choice of irradiation directions.

In regions far away from the PTV, the anisotropy changes, if the beam direction is varied [cf. Fig. 1(b)]. However, inside the PTV the anisotropy changes based on deformations of the patient geometry, which require a new dose distribution. A prediction of those variations is a prerequisite for using the anisotropy for adaptation purposes. After the superposition of beams, the anisotropy should hardly undergo variations even if the treatment technique is changed. Actually, is there a class of several techniques, which yields an identical or at least a similar anisotropy distribution inside the PTV as indicated by the two graphs for two different treatment techniques (VMAT and seven-field IMRT) in Fig. 1(a)?

As previously mentioned, variations of the anisotropy may be influenced by the specific choice of irradiation directions. Different treatment techniques as well as the rotated beam configurations of one treatment technique can be classified by means of their sensitivity to perturbations due to directional changes.

For an estimate of the maximum perturbation on one treatment technique, the rotation angle was chosen to be $\Delta\gamma = \frac{\gamma_{int}}{4}$ for an odd and $\Delta\gamma = \frac{\gamma_{int}}{2}$ for an even number of irradiation directions, assuming nearly equivalent anisotropy distributions of two opposing beams. $\gamma_{int} = \frac{360^\circ}{N}$ denotes the angle between two neighboring beams in a uniformly distributed beam configuration. To quantify variations between the anisotropy distributions A_k and A_l from plans k and l, we determine the square difference S_{kl}^2 on each voxel

$$S_{kl}^2 = (A_k - A_l)^2, \tag{4}$$

which is evaluated by structure-related statistics, e.g., the PTV:

$$S_{kl} = \sqrt{\frac{1}{N_{PTV}} \sum\nolimits_{PTV} S_{kl}^2}. \tag{5}$$

N_{PTV} denotes the number of voxels inside the PTV. However, it should be emphasized that Eq. (5) is only valid as long as the structures (PTV and OAR) are not changed, as in the course of this work.

In summary, this work addresses the following points:

- Static properties of the anisotropy inside the PTV: for plans with many beams, the anisotropy shows a decrease inside the PTV in the same way Brahme predicted a decrease in fluence.
- Similarity of anisotropy distributions: pairwise comparisons of plans establishes a class of treatment techniques whose anisotropy distributions are similar and less sensitive to a rotation of the beam directions.

3. RESULTS

3.A. The anisotropy distribution inside the PTV

For several techniques with different number N of irradiation directions, anisotropy profiles along the cross-section Y in AP direction through the PTV calculated from data for one exemplary patient are illustrated in Fig. 2. $Y = 0$ and $Y = 1$ correspond to the dorsal and the ventral PTV surface, respectively. The drawn datasets were normalized by the prescribed dose $D_{mean} = 76.2\,\text{Gy}$.

The predicted decrease $A(Y) \propto Y^\alpha$ of the anisotropy distribution with an exponent $\alpha = -\frac{1}{2}$ (indicated by the black straight line) inside the PTV could only be found for techniques with beam numbers $N \geq 7$, where three of the seven-field plans trend toward stronger exponents $\alpha < -\frac{1}{2}$ but smaller values $A(Y)$ throughout the PTV. For five-field plans, the PTV is no longer covered completely by an anisotropy value which varies from contributions in the outline.

Figure 2 depicts the anisotropy profile along an axis perpendicular to the rectum surface throughout the PTV. This figure suggests the conclusion that many-field treatment techniques ($N \geq 7$) form a universal class of techniques containing similar anisotropy distributions.

The anisotropy distributions and the confirmation of Brahme's law for real patient data depicted in Fig. 2 are an important result in terms of adaptation, since it can be seen that information on the target volume coverage and the simultaneous OAR sparing will be carried by the height of the anisotropy distribution inside the PTV. However, the illustrated profiles only reflect the special case of a distribution along a

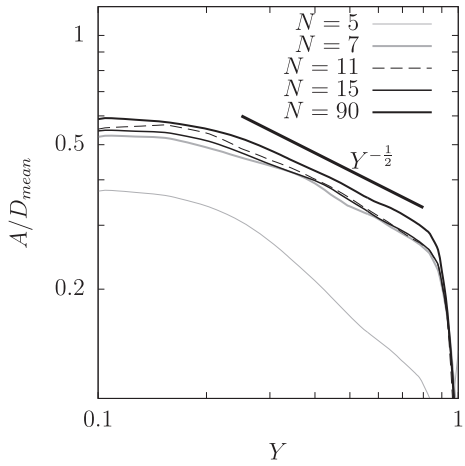

FIG. 2. Double logarithmic plot of normalized anisotropy $\frac{A}{D_{mean}}$ profiles throughout the PTV for different treatment techniques. Dorsal and ventral PTV surfaces lay at $Y = 0$ and $Y = 1$. As reference, Brahme's scaling law with an exponent $\alpha = -\frac{1}{2}$ is indicated by the thick solid line.

sagittal plane, where (in the presented cases) contributions of segments tangential to the OAR surface have their strongest contribution. The $Y^{-\frac{1}{2}}$ scaling law will only be valid in this plane and parallel to it.

3.B. Robustness of anisotropy

The definition of $\boldsymbol{A}$ depends on the choice of irradiation directions γ_n, but Fig. 2 gives the hint that a sufficiently high number of beams provides an invariant vector field at least within the PTV. Beyond a critical number of beams effects can hardly be seen. By pairwise comparison of two plans, the existence of an invariant anisotropy distribution shall be shown. Two cases will be considered: rotations of a given beam configuration and variations of the beam number.

In order to pursue the question of an invariant anisotropy distribution, a rotated plan l is generated in addition to the already existing plan k. Both plans generate an anisotropy distribution inside the PTV which is compared via the mean squared difference S_{kl} defined in Eq. (5). Normalized by the prescribed mean dose $D_{mean} = 76.2\,\text{Gy}$, S_{kl} is plotted in Fig. 3(a) for all treatment techniques.

Differences in the anisotropy distribution account for 2–3% of the prescription dose on average for the VMAT technique with irradiation from $N = 90$ control points. Plans of this technique are only rotated by 1° related to the comparatively small error. Although slightly higher, the error S_{kl} for the 15-, 11- and 7-field techniques reach similar ranges, but increasing to 5% with decreasing number of irradiation directions. Since the spatial "coverage" of one beam decreases with increasing beam number $(N = 7 : \gamma_{int} \approx 51^\circ;\ N = 11 : \gamma_{int} \approx 32^\circ;\ N = 15 : \gamma_{int} = 24^\circ)$ — leading to a rotation of $(^\circ\Delta\gamma_7 \approx 13^\circ;\ \Delta\gamma_{11} \approx 8;\ \Delta\gamma_{15} = 6^\circ)$ — a susceptibility to deviations and thus this increase of S_{kl} is expectable. It quantifies how prone a treatment technique is to deviations. For five-field plans $(\Delta\gamma_5 = 18^\circ)$, the values S_{kl} reach clearly enhanced ranges of $\frac{S_{kl}}{D_{mean}} \approx 9\%$ indicating that original and rotated beam direction lose their correlation and segments potentially change their task in terms of plan generation.

The same pairwise comparison may be executed for different treatment techniques with different beam numbers k and l on the same target volume. The total of five treatment techniques result in an off-diagonal 5×5-matrix, whose entries of the upper triangular are illustrated in Fig. 3(b) normalized by the prescribed mean dose D_{mean}. The boxplots illustrate the statistics for the ten compared plans. Again, it turns out that all treatment techniques generate an error of around $\frac{S_{kl}}{D_{mean}} = 2 - 3\%$. Only the five-field distributions differ clearly in a range from $\frac{S_{kl}}{D_{mean}} = 10\%$ up to 20%.

In conclusion, it was observed that a class of treatment techniques exists that is similar in their anisotropy distribution. VMAT as well as 15-field and 11-field IMRT plans can confidently be included into this class. Also, seven-field plans do not seem to considerably vary from the plans mentioned above, but due to deviations of approximately 5% and higher in the rotated plans this treatment technique should be excluded. The results reflect the fact, that seven-field IMRT

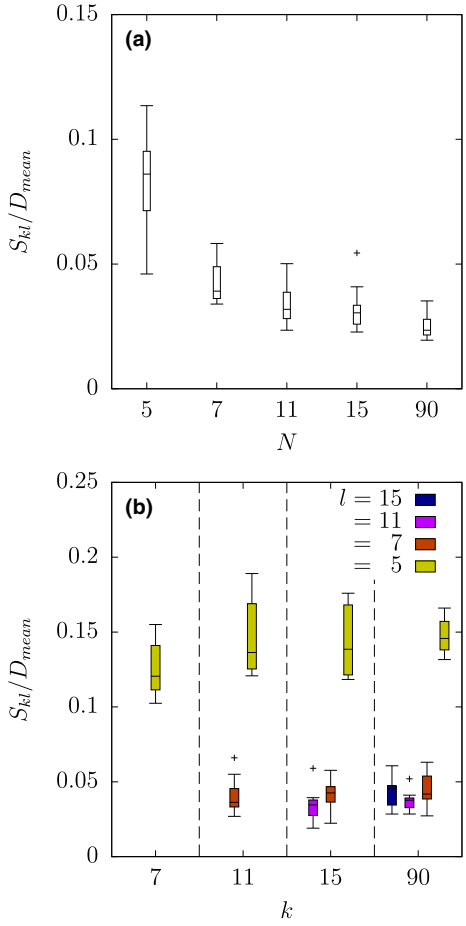

FIG. 3. (a) Mean square difference S_{kl} inside the PTV between an original plan k and a rotated plan l for the same number of beams N (treatment technique). (b) Comparison between the treatment techniques. k and l represent the respective number of irradiation directions. The data was normalized by the prescribed dose D_{mean}. Crosses indicate outliers, which have a distance from the median larger than 1.5 times the interquartile range. [Color figure can be viewed at wileyonlinelibrary.com]

techniques may generate good plans in individual cases, while they are sometimes restricted by geometrical limits which cannot be handled by reduced beam numbers. This discrimination can be seen even more in the results for five-field plans, which do not reach practical application.

In terms of plan adaptations, the robustness of anisotropy plays an important role. Let us emphasize that only the combination of both diagrams in Fig. 3 illustrates the robustness of anisotropy distributions in terms of low deviations.

In summary, we determine similar deviations when comparing two treatment techniques, with no significant variations except of the five-field technique, but under rotation of plans the robustness decreases with a decrease in beams.

4. DISCUSSION

The anisotropy, as defined by Eqs. (1) and (2), is a quantity independent from the choice of treatment technique. It can be computed for any IMRT and VMAT plan. Brahme predicted a necessary fluence profile with a $F(r) \propto r^{-\frac{1}{2}}$ inside the PTV adjacent to the *OAR*. In the vicinity of an OAR, it is

approximately proportional to the anisotropy.[14] Anisotropy profiles in a cross-section through the isocenter show curves with similar scaling law throughout the PTV, to a certain range independent from the treatment technique. The calculations for the fluence presented by Brahme[17] and also for the anisotropy performed by Bratengeier[10] were based on rotational symmetric target volumes. Thus, deviations from this scaling in "real" patient data (cf. Fig. 2) may result from asymmetries in the position and shape of the PTV relative to the isocenter, cross-section line.

4.A. Recommendations for the technique choice

In addition to a fundamental description of the anisotropy inside the PTV (1.1 in Table I), this work aimed at finding out whether a class of treatment techniques exists yielding similar anisotropy distributions. Therefore, the influence of irradiation directions on the anisotropy was studied (1.2.1 in Table I). Here, a decrease in plan quality for decreasing numbers of irradiation directions should be taken into account (cf. Appendix A), since the anisotropy is considered as an indicator for requirements on organ sparing as well as target volume coverage. Correspondingly, the anisotropy distribution only is subject to small variations for a minimum of irradiation directions. If the number of beams falls below a critical value (in the presented prostate cases: $N < N_c = 7$), an accurate target coverage gets lost and the anisotropy distribution varies significant from multifield cases (cf. Figs. 2 and 3). The critical number N_c is case dependent, thus, for adaptation purposes in more complex prostate cases more than seven beams could be recommended, even if the standard of a VMAT technique is not available.

In addition to the pairwise comparison of treatment techniques, the anisotropy distribution was checked by calculation on rotated plans and comparison with the original plan. From this study, the robustness of each treatment technique can be classified (1.2.2 in Table I). Multiple beam techniques $(N \geq 7)$ were less sensitive to perturbations.

The anisotropy has proven to be a robust quantity for many-beam techniques, which is an essential condition in terms of adaptation. Further necessary conditions consist in the sensitivity to different beam weightings as well as different anatomic conditions. Where effects of deformations have already been seen,[14] a quantification of the anisotropy for different grades of organ sparing will be the topic of further publications in preparation. Then, deforming the anisotropy distribution will result in special rules for the segment adaptation along the new structures. Both steps have been performed quantitatively for a cylindrical symmetric situation and qualitatively for prostate and head and neck cases.[14] For the cylindrical symmetric situation, a strong correlation of anisotropy and segment shape has been shown.

The investigative endpoint is the development of an algorithm for leaf adaptations in dependence of the anisotropy distribution. If successful, this can be considered an upgrade of conventional aperture based adaptation, avoiding shortcomings for concave–convex PTV-OAR-constellations.[12]

5. CONCLUSIONS

The results reveal a class of techniques yielding similar distributions of the anisotropy of dose distributions defined in the radiotherapy treatment of prostate carcinomas. Basic requirements needed for the adaptation of segments have been demonstrated on real patient data. Strong gradients which carry information on target volume coverage as well as on OAR sparing are included within the PTV. Many-beam techniques are recommended under the aspects of plan quality, reproducibility of anisotropy and robustness.

The presented results open the way for detailed investigations of the anisotropy distribution in response to controlled virtual and real organ deformations. Organ deformations and replanning should reveal rules for the identification of leaf opening positions leading to suitable *OAR* tangential dose contributions.

ACKNOWLEDGMENTS

The authors thank Florian Exner for his help with the PINNACLE3 handling and Kostyantyn Holubyev for productive discussions. We also want to express our gratitude to Linda Wack and Gary Razinskas for finding and correcting our mistakes in English language.

CONFLICTS OF INTEREST

The authors have no conflicts of interest to disclose.

APPENDIX A

PLAN GENERATION AND PLAN QUALITY

A total of 10 standard prostate cases were included in this study. In each primary CTs for standard prostate cases, the boost surrounded by the PTV[17] and the two OARs, rectum and bladder, were contoured. A VMAT plan and various IMRT plans (5-, 7-, 11-, 15-fields, optimized in the DMPO mode of PINNACLE3 version 9.10) were generated to fulfill the clinical constraints (PTV boost: $D_{mean} = 76.2\,\text{Gy}$, $\sigma \leq 2.5\,\text{Gy}$, $D_{95} \geq 74\,\text{Gy}$, $D_{99} = 69.9\,\text{Gy}$; PTV: $D_{95} \geq 60.1\,\text{Gy}$, $D_{99} \geq 56.1\,\text{Gy}$; bladder: $D_{10} \leq 60\,\text{Gy}$; femoral heads: $D_{05} \leq 40\,\text{Gy}$; and outline-(PTV + 2): $D_{max} \leq 66.6\,\text{Gy}$) in 33 fractions. A further criterion for rectum sparing is the condition that the dose at any point of the dorsal rectum wall shall not exceed 30% of PTV boost D_{95} (evaluated in the isocentric sagittal plane). We further aim at reaching PTV-(PTV-rectum): $D_{05} \leq 72.4\,\text{Gy}$, but this criterion is no real constraint and consequently was failed by all planned techniques. Table II lists to what extent these requirements were achieved by the different treatment techniques. It is evident that the number of irradiation directions influences the plan quality

TABLE II. Plan quality assessment for all treatment techniques.

Volume	Required	Value	N = 5	N = 7	N = 11	N = 15	N = 90 (VMAT)
Boost	D_{mean} (Gy)	76.2 ± 1%	76.0 ± 0.2	76.0 ± 0.1	76.0 ± 0.1	76.0 ± 0.1	76.0 ± 0.1
	σ (Gy)	<2.5	1.4 ± 0.2	1.1 ± 0.1	1.1 ± 0.1	1.1 ± 0.1	1.0 ± 0.1
	D_{95} (Gy)	74.0 ± 2%	73.3 ± 0.4	73.7 ± 0.4	73.8 ± 0.3	73.7 ± 0.3	73.9 ± 0.4
	D_{99} (Gy)	>70.0	71.6 ± 0.7	72.3 ± 0.5	72.5 ± 0.4	72.3 ± 0.5	72.7 ± 0.4
	D_{01} (Gy)	<80.0	78.7 ± 0.5	77.9 ± 0.2	77.8 ± 0.3	77.9 ± 0.2	77.6 ± 0.2
PTV Boost	D_{95} (Gy)	60.1 ± 2%	58.7 ± 0.8	59.8 ± 0.7	60.0 ± 0.7	60.0 ± 0.7	60.2 ± 0.6
	D_{99} (Gy)	>56.1	55.6 ± 1.3	57.4 ± 1.1	57.3 ± 1.2	57.7 ± 1.1	58.1 ± 0.8
Outl-(PTV + 2)	D_{max} (Gy)	<66.6	65.8 ± 6.2	61.2 ± 6.8	58.3 ± 3.9	55.1 ± 3.3	54.8 ± 3.9
Bladder	D_{10} (Gy)	<60.0	54.1 ± 10.1	53.1 ± 11.4	52.9 ± 11.3	53.0 ± 11.7	52.6 ± 11.4
Fem. H. l	D_{05} (Gy)	<40.0	44.0 ± 1.7	37.3 ± 2.7	38.8 ± 1.3	39.0 ± 1.8	35.8 ± 2.6
Fem. H. r	D_{05} (Gy)	<40.0	43.6 ± 2.2	35.5 ± 3.1	37.6 ± 2.8	38.0 ± 3.7	35.5 ± 3.3
PTV-(PTV-rect)	D_{05} (Gy)	<72.4	72.6 ± 0.8	73.0 ± 0.9	73.0 ± 0.9	73.0 ± 0.8	72.8 ± 1.0
Rectum	Dorsal wall	<0.3 D_{95}	70%	70%	80%	80%	90%
Av. Number of fails per plan			4.6	1.9	1.8	1.8	1.2
Rectum	V_{95} (cm^3)		0.0 ± 0.0	0.1 ± 0.1	0.1 ± 0.2	0.0 ± 0.1	0.2 ± 0.0
	V_{80} (cm^3)		6.8 ± 2.3	8.6 ± 2.2	8.7 ± 2.6	9.0 ± 3.1	9.1 ± 2.3
	V_{50} (cm^3)		27.5 ± 6.9	26.7 ± 7.0	26.7 ± 6.9	26.8 ± 7.1	26.2 ± 7.1
COV			2.3 ± 0.5	1.4 ± 0.2	1.2 ± 0.1	1.2 ± 0.1	1.00

List of achieved clinical constraints in the dose–volume histogram: for every treatment technique, the mean and standard deviation of 10 plans is given together with the average number of fails per plan. In particular those plans, which yield robust anisotropies, satisfy the clinical constraints in a sufficient way.
An additional parameter was calculated in the planning system: the sum of weighted quadratic deviations from set points defining the desired course in the dose–volume histogram (DVH) like the minimum of a harmonic potential. In Pinnacle3, this value is available as composite objective value (COV) and is minimized during the optimization process. If both, all plans were subject to the same conditions, that is, the same parameter sets were used and a sufficient number of representative DVH points were used the COV serves as indicator for that technique with the smallest deviations from the desired DVH course.[16,17] For this study, all COVs were normalized to the COV of the volumetric modulated arc therapy plan.

particularly if the considered number of beams is chosen too small.

[a)]Author to whom correspondence should be addressed. Electronic mail: greber_j@ukw.de.

REFERENCES

1. Bzdusek K, Friberger H, Eriksson K, Hardemark B, Robinson D, Kaus M. Development and evaluation of an efficient approach to volumetric arc therapy planning. *Med Phys*. 2009;36:2328–2339.
2. Otto K. Volumetric modulated arc therapy: IMRT in a single gantry arc. *Med Phys*. 2008;35:310–317.
3. Wilbert J, Baier K, Hermann C, Flentje M, Guckenberger M. Accuracy of real-time couch tracking during 3-dimensional conformal radiation therapy, intensity modulated radiation therapy, and volumetric modulated arc therapy for prostate cancer. *Int J Radiat Oncol Biol Phys*. 2013;85:237–242.
4. Ravkilde T, Keall PJ, Grau C, Hoyer M, Poulsen PR. Fast motion-including dose error reconstruction for VMAT with and without MLC tracking. *Phys Med Biol*. 2014;59:7279–7296.
5. Wu QJ, Thongphiew D, Wang Z, et al. On-line re-optimization of prostate IMRT plans for adaptive radiation therapy. *Phys Med Biol*. 2008;53:673–691.
6. Mohan R, Zhang X, Wang H, et al. Use of deformed intensity distributions for on-line modification of image-guided IMRT to account for interfractional anatomic changes. *Int J Radiat Oncol Biol Phys*. 2005;61:1258–1266.
7. Crijns W, Defraene G, Van Herck H, et al. Online adaptation and verification of VMAT. *Med Phys*. 2015;42:3877–3891.
8. Kontaxis C, Bol GH, Lagendijk JJ, Raaymakers BW. A new methodology for inter- and intra-fraction plan adaptation for the MR-linac. *Phys Med Biol*. 2015;60:7485–7497.
9. Kontaxis C, Bol GH, Lagendijk JJ, Raaymakers BW. Towards adaptive IMRT sequencing for the MR-linac. *Phys Med Biol*. 2015;60:2493–2509.
10. Prior P, Chen X, Botros M, et al. MRI-based IMRT planning for MR-linac: comparison between CT- and MRI-based plans for pancreatic and prostate cancers. *Phys Med Biol*. 2016;61:3819–3842.
11. Kontaxis C, Bol GH, Stemkens B, et al. Towards fast online intrafraction replanning for free-breathing stereotactic body radiation therapy with the MR-linac. *Phys Med Biol*. 2017;62:7233–7248.
12. Bratengeier K, Oechsner M, Gainey M. Methods for monitor-unit-preserving adaptation of intensity modulated arc therapy techniques to the daily target – a simple comparison. *Med Phys*. 2012;39:713–720.
13. Holubyev K, Gainey M, Bratengeier K, Polat B, Flentje M. Generation of prostate IMAT plans adaptable to the inter-fractional changes of patient geometry. *Phys Med Biol*. 2014;59:1947–1962.
14. Bratengeier K, Holubyev K. Anisotropy of dose contributions – an instrument to upgrade real time IMRT and VMAT adaptation? *Med Phys*. 2016;43:5826.
15. Bratengeier K, Gainey MB, Flentje M. Fast IMRT by increasing the beam number and reducing the number of segments. *Radiat Oncol*. 2011;6:170.
16. Brahme A, Roos JE, Lax I. Solution of an integral equation encountered in rotation therapy. *Phys Med Biol*. 1982;27:1221–1229.
17. Guckenberger M, Lawrenz I, Flentje M. Moderatly hypofractionated radiotherapy for localized prostate cancer. *Strahlenther Onkol*. 2014;190:48.